Theoretical Investigation of the Fe^+-Catalyzed Oxidation of Acetylene by N_2O

Lianming Zhao,[†] Yong Wang,[§] Wenyue Guo,*[,†] Honghong Shan,*[,‡] Xiaoqing Lu,[†] and Tianfang Yang[†]

College of Physics Science and Technology, College of Chemistry and Chemical Engineering, and College of Electromechanical Engineering, China University of Petroleum, Dongying, Shandong 257061, People's Republic of China

Received: January 18, 2008; Revised Manuscript Received: March 13, 2008

The gas-phase Fe^+-mediated oxidation of acetylene by N_2O on both sextet and quartet potential energy surfaces (PESs) is theoretically investigated using density functional theory. Geometries and energies of all the stationary points involved in the catalytic reaction are located. For the catalytic cycles, the crucial step is the initial N_2O reduction by Fe^+ to form FeO^+, in which a direct O-abstraction mechanism is located on the sextet PES, whereas the quartet pathway favors a N−O insertion mechanism. Spin inversion moves the energy barrier for this process downward to a position below the ground-state entrance channel. The second step of the catalytic cycles involves two mechanisms corresponding to direct hydrogen abstraction and cyclization. The former mechanism accounts for the ethynol formation with the upmost activation barrier below the entrance channel by about 5 kcal/mol. The other mechanism involves a "metallaoxacyclobutene" structure, followed by four possible pathways, i.e., direct dissociation, C−C insertion, C-to-O hydrogen shift, and/or C-to-C hydrogen shift. Among these pathways, strong exothermicities as well as energetically low location of the intermediates suggest oxidation to ketene and carbon monoxide along the C-to-C hydrogen shift pathway is the most favorable. Reduction of the CO loss partner $FeCH_2^+$ by another N_2O molecule constitutes the third step of the catalytic cycles, which contains direct abstraction of O from N_2O giving $OFeCH_2^+$, intramolecular rearrangement to form Fe^+-OCH_2, and nonreactive dissociation. This reaction is also energetically favored considering the energy acquired from the initial reactants.

1. Introduction

The catalytic reaction involving transition metal ions and their oxides is of paramount interest due to its enormous practical importance in industrial and environmental processes.[1] In this respect, gas-phase studies can provide a wealth of insight into elementary steps of various catalytic reactions and characterize the reaction intermediates.[2–4] Because nitrous oxide has been identified as an ozone-depletion agent and one of the greenhouse gases,[5] many of the studies concentrated on the reduction of N_2O in the gas phase.[6,7] Owing to the low N_2-oxygen affinity ($OA(N_2) = 40$ kcal/mol[8]), N_2O is a useful O-atom donor for producing transition metal oxide cation, which is a key intermediate in selective catalytic oxidation mediated by transition metal ions. The gas-phase transition metal ion-catalyzed oxidations of small molecules by N_2O have been investigated extensively, and Fe^+ was found to present a good catalytic property in these reactions.[4,9–18] For example, the landmark experiments by Kappes and Staley in 1981 demonstrated that although transition metal oxide cations could be produced in N_2O reaction with Ti^+, Zr^+, V^+, Nb^+, Cr^+, and Fe^+, catalytic oxidation cycles involving M^+ and MO^+ were only observed for Fe^+ when CO, C_2H_2, and other simple oxygen acceptors were added.[9] A further ion-beam experiment by Armentrout et al. suggested that Fe^+ reaction with N_2O to afford FeO^+ exhibits no activation energy.[6a] Due to the high reactivity, Fe^+ that mediates O-atom transfer to olefins also catalyzes isomerizations of the epoxides formed, to afford the energetically more stable aldehydes or ketones.[16] Schwarz and co-workers have pointed out that Fe^+ could selectively catalyze the CH_4, C_2H_6, and C_6H_6 oxidation by N_2O, producing methanol, alcohol/acetaldehyde, and phenol, respectively.[4,10–13,16] Selected ion flow tube (SIFT) experiments by Bohme and co-workers demonstrated that the $Fe^+/N_2O/CO$ catalytic cycle is not poisoned by N_2O, because $FeO(N_2O)_n^+$ ($n = 0-3$) remain reactive at least up to $n = 3$.[17,18]

From the theoretical point of view, in order to elucidate the reaction mechanisms and determine the activation barriers, very recently, the Fe^+-catalyzed oxidation of CO by N_2O has been under detailed consideration.[18,19] Blagojevic et al.[18] have reported the sextet potential energy surface (PES) using the B3LYP/6-311+G(d) protocol, in which the FeO^+ oxide was found to be generated from the OFe^+N_2 precursor through an $O-N_2$ insertion transition state. Subsequently, coordination of $Fe^+O\cdots CO$ is followed by rearrangement to $Fe^+\cdots OCO$ and rupture of the metal−oxygen bond, giving Fe^+ and CO_2. The rate-determining step in this catalytic cycle is the N−O insertion process (energy barrier: 0.9 kcal/mol).[18] Interestingly, by using the B3LYP method in conjunction with the DZVP(opt) set of Chiodo et al.,[20] a direct O-abstraction mechanism where the O atom of N_2O is directly abstracted by Fe^+ via an energy barrier of 0.7 kcal/mol was presented to elucidate the formation of FeO^+ when the crossings between the sextet and quartet PESs were considered; the subsequent FeO^+ reduction by CO could occur via a barrierless process, in which CO moves close to the FeO^+ oxide from the oxygen side.[19] In addition, the oxidation mechanisms of H_2, CH_4, C_6H_6, and several other organic substrates by FeO^+ have also been theoretically studied.[21–25] The low reactivity of FeO^+ toward molecular hydrogen was

* To whom correspondence should be addressed. E-mail: wyguo@hdpu.edu.cn (W.G.), shanhh@hdpu.edu.cn (H.S.).
† College of Physics Science and Technology.
‡ College of Chemistry and Chemical Engineering.
§ College of Electromechanical Engineering.

10.1021/jp800511h CCC: $40.75
Published on Web 05/31/2008

SCHEME 1

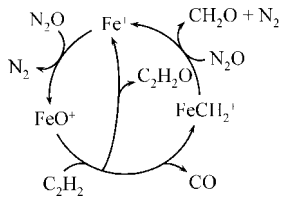

found to be due to the extreme inefficiency of PESs crossing before the H−H activation transition state.[21] Methane oxidation by FeO^+ occurs via a direct H abstraction by the oxide, followed by methyl migration giving methanol, and spin inversion decreases the rate-limiting barrier height from 31.1 to 22.1 kcal/mol at the B3LYP level.[22] The mechanism of further FeO^+-mediated oxidations of methanol to formaldehyde, formaldehyde to formic acid, and formic acid to carbon dioxide was also discovered by Yoshizawa and co-workers.[23] The overall reaction from methane to carbon dioxide was found to be exothermic by 117.9 kcal/mol without any high barriers after the methanol formation. Yoshizawa and co-workers suggested that the major reaction pathway of direct oxidation of benzene by FeO^+ to phenol favors a nonradical mechanism to form a hydoroxo intermediate, $HO-Fe^+-C_6H_5$, via H-atom abstraction with a four-member-ring transition state as the rate-determining barrier.[22e,24]

Nevertheless, to the best of our knowledge, so far, quantum-chemical studies of the hydrocarbons oxidation by FeO^+ are mainly limited to H−H and C−H activation and rather scarce for C−C activation. In this article, we reported a comprehensive theoretical investigation of the Fe^+-catalyzed N_2O reduction with one of the simplest hydrocarbons, acetylene. One interesting reason for this study is it may involve both C−H and C−C activations. The other reason is it contains both two-step and three-step catalytic cycles for the respective products (Scheme 1), compared to that only a two-step cycle is involved in the analogous reaction with CO.[9] First, the O-atom transfer generates FeO^+, which acts as a "monooxygenase" for the hydrocarbon oxidation (reaction 1). Then, FeO^+ reaction with acetylene in part directly gives Fe^+ (reaction 2) but also eliminates CO producing $FeCH_2^+$ (reaction 3). Further reaction of $FeCH_2^+$ with N_2O regenerates Fe^+ (reaction 4). After the catalytic cycles complete, C_2H_2O, CH_2O, CO, and N_2 are formed (reaction 5).[9]

$$2N_2O + 2Fe^+ \rightarrow 2FeO^+ + 2N_2 \quad (1)$$

$$FeO^+ + C_2H_2 \rightarrow Fe^+ + C_2H_2O \quad (2)$$

$$FeO^+ + C_2H_2 \rightarrow FeCH_2^+ + CO \quad (3)$$

$$FeCH_2^+ + N_2O \rightarrow Fe^+ + N_2 + CH_2O \quad (4)$$

$$2C_2H_2 + 3N_2O \rightarrow C_2H_2O + CH_2O + CO + 3N_2 \quad (5)$$

Our main aim is to elucidate the reaction mechanisms and determine the activation barriers useful to give insight into kinetic aspects. This includes a complete description of PESs of all possible pathways on both the sextet and quartet PESs for the full catalytic oxidation cycles.

2. Computational Details

All computations were performed at the hybrid density functional B3LYP[26] using the GAUSSIAN 03 program package.[27]

TABLE 1: Bond Dissociation Energies and Excitation Energies (in kcal/mol) at 0 K Determined by Calculations and Experiments

species	calcd[a,b]	expt
$^5[Fe^+-H]$	55.8 (8.2 ± 1.4)	47.6 ± 1.4[c]
$^5[Fe^+-OH]$	82.9 (0.3 ± 4)	82.6 ± 4[d]
$^4[Fe^+-OH_2]$	29.7 (−1.0 ± 1.2)	30.7 ± 1.2[e]
$^6[Fe^+-O]$	76.9 (−3.1 ± 1.4)	80.0 ± 1.4[f]
$^4[Fe^+-CO]$	33.4 (2.1 ± 1.8)	31.3 ± 1.8[g]
N_2-O	41.1 (1.05 ± 0.02)	39.95 ± 0.02[h]
$^5[Fe^+-CH_3]$	59.7 (5.1 ± 1.1)	54.6 ± 1.1[i]
$^4[Fe^+-CH_2]$	89.8 (6.8 ± 4)	83.0 ± 4[j]
$^4[Fe^+-OCH_2]$	33.9 (1.0 ± 1.7)	32.9 ± 1.7[d]
$^4[Fe^+-N_2]$	13.4 (0.7 ± 0.9)	12.7 ± 0.9[k]
Fe^+ ($^4F \leftarrow {}^6D$)	12.5 (6.7)	5.8[l]

[a] The B3LYP/DZVP(opt+3f)+6-311+G(2d,2p) level. [b] Values in the parentheses are error bars for the calculated BDEs, obtained by subtracting the experimental values from the calculated BDEs. [c] Ref 31. [d] Ref 32. [e] Ref 33. [f] Ref 34. [g] Ref 35. [h] Ref 8. [i] Ref 36. [j] Ref 37. [k] Ref 38. [l] Ref 39.

We chose the DZVP(opt) set of Chiodo et al.,[20] supplemented with three sets of uncontracted pure angular momentum *f* functions to describe Fe^+ ion (noticed as DZVP(opt+3f)), and the 6-311++G(2d,2p) basis set[28] for nonmetal atoms to fully optimize the structure of all species involved in the title reaction. The DZVP(opt) set built up by Chiodo et al. has presented a good reliability for density functional B3LYP method in predicting transition metal ion ground- and excited-state order and splitting.[19,20]

The harmonic vibrational frequencies of the optimized stationary points were calculated at the same level to estimate the zero-point energies (ZPE) that are included in all cited energies and to characterize stationary points on the PESs as local minima or transition states. Intrinsic reaction coordinate (IRC) calculations were performed to identify the pathways between transition states and their connecting minima. The calculation method STABLE[29] was used everywhere to ensure the wave function of stationary points to be tested. Natural bond orbital (NBO)[30] analyses were carried out to characterize the bonds and the interactions inside the relevant species.

3. Results and Discussion

In the following sections, we will first establish the accuracy that is expected from the chosen level of theory for the $Fe^+/N_2O/C_2H_2$ system. Then, we will examine the title reaction in detail, including geometries of all relevant stationary points and PES profiles for all the catalytic steps. For simplicity, calculated total energies, ZPEs as well as $\langle S^2 \rangle$ values for all the species involved in the reaction are given as Supporting Information (see Table S1).

3.1. Calibration. To evaluate the reliability of the level of theory employed, we compare the experimentally known thermochemical data with the results from the B3LYP approach. Table 1 collects the theoretically predicted bond dissociation energies (BDE) and the most reliable experimental data for some relevant species.[8,31–39] Given in the parentheses are error bars for the calculated BDEs, which are obtained by subtracting the experimental values from the calculated ones.

As shown in Table 1, the calculations reproduce the experimental BDEs well in most cases except $^5[Fe^+-H]$, $^5[Fe^+-CH_3]$, and $^4[Fe^+-CH_2]$. Although the difference of the calculated excitation energy of Fe^+ (^4F, $3d^7 \leftarrow {}^6D$, $3d^64s^1$) with the experimental gap value is not small (12.5 vs 5.8 kcal/mol),[39] the basis set used here can reproduce the correct order of the

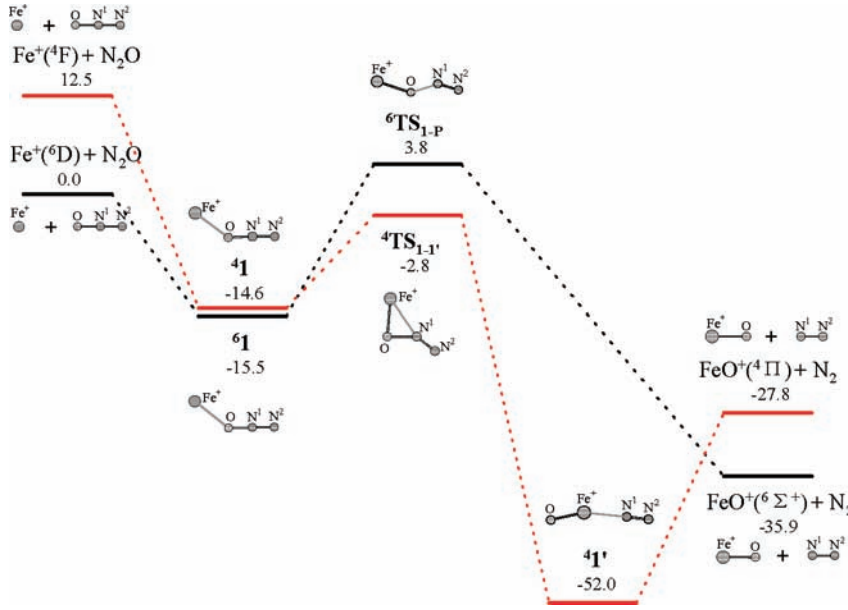

Figure 1. Energy profile for N_2O reduction mediated by Fe^+. Numbers refer to the relative stabilities (in kcal/mol) with respect to the separated reactants of $N_2O + Fe^+(^6D)$ evaluated at the B3LYP/DZVP(opt+3f)+6-311+G(2d,2p) level including ZPE corrections. Scaling factor for the ZPE is 0.961.

electronic states. Furthermore, one obvious performance of the presently used basis set is it can give a good prediction of the oxygen affinity for iron ion, which is only underestimated by 3.1 kcal/mol from the experimental value (see Table 1), compared to an underestimation of about 10 kcal/mol at the B3LYP/DZVP(opt) level.[19] This better prediction of the oxygen affinity value is expected to give a more accurate reaction energy of the first step of the catalytic cycles studied (reaction 1).

3.2. N_2O Reduction Mediated by Fe^+. The N_2O reduction mediated by Fe^+ has been theoretically studied by other authors.[18,19] Blagojevic et al.[18] reported a N−O insertion mechanism to describe the sextet PES using the B3LYP/6-311+G(d) protocol. Rondinelli et al.[19] found that the reaction occurs through a direct O-abstraction mechanism on both sextet and quartet PESs at the B3LYP/DZVP(opt) level of theory. In our calculations (see Figure 1 and Supporting Information Figure S1), the direct O-abstraction mechanism is located on the sextet PES, whereas the quartet pathway favors the N−O insertion mechanism. The difference of the mechanisms concerns the structures of the relevant transition states in different spin states. As shown in Figure 1 and Supporting Information Figure S1, the transition state on the quartet PES (^{4}**TS$_{1-1'}$**) is featured by a three-member-ring structure with the Fe^+−O−N^1 angle of 85.3° and the Fe^+−N^1 distance of 2.211 Å, indicating a relatively strong interaction of Fe^+ with O−N_2 bond, which favors the N−O insertion. For its sextet counterpart (**^{6}TS$_{1-P}$**), however, the facts that the metal attaches O from the end side as reflected by the Fe^+−O−N^1 angle (141.2°), as well as the shortening of the Fe^+O bond is accompanied by the stretch of the ON^1 bond suggest it is really the exit transition state for the direct ejection of N_2. IRC calculations confirm these aspects.

The rate-limiting barrier for the N_2O reduction has been reported to be 0.9 kcal/mol by Blagojevic et al.[18] and 0.7 kcal/mol by Rondinelli et al. considering the two-state reactivity phenomenon.[19] However, by us it is located at 2.8 kcal/mol below the sextet entrance channel if the two-state reactivity phenomenon is taken into account, according with the ion-beam experimental results that reaction of Fe^+ with N_2O giving FeO^+ exhibits no activation energy.[6a] Hence, spin inversions, which occur immediately before the transition states and the exit channels, seem to be the rate-limiting step in this reaction.

The overall reaction is calculated to be exothermic by 35.9 kcal/mol, which is 5.0 kcal/mol higher than that of Rondinelli et al. (30.9 kcal/mol).[19] The difference of the exothermicity values accords well with the difference of the Fe^+-oxygen affinity calculated by us from that by Rondinelli et al.[19] Because, as mentioned above, the oxygen affinity value calculated at the presently used level is closer to the experimental value, we are confident that the PES presented by us is more exact than that of Rondinelli et al.[19]

3.3. C_2H_2 Oxidation by FeO^+. Acetylene oxidation by FeO^+ could result in two parallel neutral eliminations corresponding to CO and C_2H_2O.[9] In the following, all possible mechanisms for the loss of CO and three possible C_2H_2O isomers, i.e., ketene (CH_2CO), ethynol (CHCOH), and formylcarbene (CHCHO), will be considered. The other possible isomer of C_2H_2O, oxirene, which has not yet been observed experimentally and has been located as either a minimum or a transition state at various levels of theory previously,[40–42] is computed as a transition state with an imaginary frequency of 137*i* cm^{-1} at the B3LYP/6-311++G(2d,2p) level. Hence, the formation of this isomer will not be included in the discussion.

3.3.1. Encounter Association of FeO^+ with Acetylene. Acetylene oxidation by FeO^+ starts with the association of FeO^+ with C_2H_2 (reaction 2). Although the sextet entrance channel is energetically lower than its quartet analogue, the sextet and quartet encounter species are almost degenerate, lying at about 42.5 kcal/mol below the separated reactants of $FeO^+(^6\Sigma^+) + C_2H_2$. Optimized geometries as well as selected structural parameters for the complex are shown in Figure 2. In both cases, the oxide attaches the two acetylenic C atoms simultaneously through the metal with the difference that the Fe^+O bond locates along the C_2 axis in **^{6}2** (C_{2v}), whereas the quartet association (C_s) favors an out-of-plane location of the Fe^+O bond (the dihedral angle of Fe^+O with the Fe^+C_2 plane is 96.6°). This association results in elongation of the C−C bond as well as distortion of the C−C−H angle (especially for the quartet species).

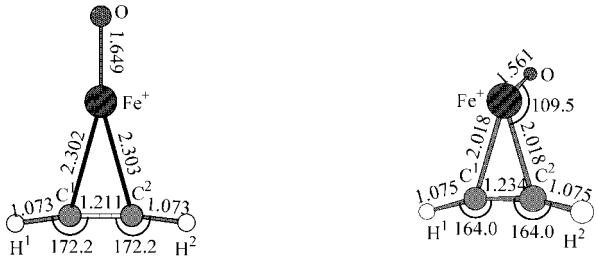

^{6}2 (C_{2v}) **^{4}2** (C_s)

Figure 2. Optimized geometries and selected structural parameters (in angstroms and deg) for the OFe^+−acetylene complex in its sextet (left) and quartet (right) states at the B3LYP/DZVP(opt+3f)+6-311+G(2d,2p) level of theory.

In order to clarify why association of C_2H_2 with the quartet FeO^+ stabilizes the system to a larger extent than that with the sextet analogue, we analyze Mulliken atomic spin densities and natural orbitals for the relevant species, and the results are given in Supporting Information Tables S2−S4, respectively (see the Supporting Information). For free $^6FeO^+$, values of Mulliken atomic spin densities on Fe^+ and O are nearly 4 and 1, respectively (see Supporting Information Table S2). NBO analysis shows this situation favors formation of a doubly occupied σ and two β singly occupied π binding orbitals between the constituent atoms (see Supporting Information Table S3). In the quartet state of FeO^+, however, the respective Mulliken atomic spin densities of 2.35 and 0.65 on Fe^+ and O favor one more π binding orbital occupied doubly in addition to the same bonding situations as in the sextet oxide (see Supporting Information Table S3).

Complex with C_2H_2 in the sextet state results in almost no change of Mulliken atomic spin densities on Fe^+ and O (3.94 and 1.08). NBO analysis indicates that the complexation process does not change the bonding situations of both constituent entities and the complex is stabilized by the classical Dewar−Chatt−Duncanson mechanism,[43] i.e., donation of $3d(Fe^+) \rightarrow \pi^*(CC)$ and back-donations of $\pi(CC) \rightarrow \sigma^*(Fe^+O)$ and $4s(Fe^+)$ ($\Delta E^{(2)} = 39.9$ kcal/mol; see Supporting Information Table S4). For the quartet species (**^{4}2**), however, although total spin densities of the Fe^+O entity do not change obviously, relatively large changes of spin densities are observed for the individual atoms (2.78/0.34 for Fe^+/O). It is important to note that this complexation results in rupture of the $\alpha-\pi(Fe^+O)$ orbital, though the bond is strengthened as mirrored by the bond length (1.561 compared to 1.690 Å in free $^4FeO^+$). The larger stabilization in this state is attributed to donor−acceptor interactions. Indeed, in this case, in addition to the stronger donor−acceptor interactions between C_2H_2 and FeO^+ ($\Delta E^{(2)} =$ 103.9 kcal/mol), relatively large electron donations are also found in the FeO^+ entity (see Supporting Information Table S4), explaining the strengthening of the Fe^+-O bond as well as the stabilization of the state.

Once the association is reached, two mechanisms noticed as direct hydrogen abstraction and cyclization could be followed for the oxidation reaction.

3.3.2. Direct Hydrogen Abstraction. The PES together with schematic structures involved in the sextet and quartet pathways of the channel is shown in Figure 3. Information about these relevant species is given in Supporting Information Figure S2. Initially, direct C^1-to-O H shift mediated by a $Fe^+-C^1-C^2$ scissor vibration could carry species **2** to the $(HO)Fe^+(CCH)$ complex (**3**), which in its sextet and quartet states lies at −57.6 and −44.3 kcal/mol with respect to the energetic zero, respectively. One obvious feature of the new species is the dicoordination of the metal center. Spin densities for the quartet species locate mainly on Fe^+ (3.09; see Supporting Information Table S2), and the metal forms a doubly occupied σ binding orbital with C^1 as well as a α singly occupied σ binding orbital with O (see Supporting Information Table S3). For the ground complex (**^{6}3**), however, spin densities are found to locate mainly on Fe^+ (4.17), C^1 (0.45), and O (0.48). Rupture of the β-spin $\pi(CC)$ and $\sigma(Fe^+C^1)$ as well as α-spin $\sigma(Fe^+O)$ orbitals is accompanied by the population of both β-spin $\pi(Fe^+O)$ and $\sigma(Fe^+O)$ orbitals, which favors relatively strong electron donations of $4p3d^{10.76}(Fe^+) \rightarrow 2p(C^1)$, $2s2p^{1.06}(O) \rightarrow 4s3d^{3.02}(Fe^+)$, and $2p(C^1) \rightarrow 2p(C^2)$ (see Supporting Information Table S4) and stabilizes the system largely. This possibility involves a four-member-ring transition state (**TS_{2-3}**) that lies at −4.9 kcal/mol for the sextet and 5.7 kcal/mol for the quartet.

A subsequent coupling of the end ligands in species **3** could result in Fe^+−ethynol adduct **4**, the direct precursor of ethynol-loss products. A striking feature of the sextet Fe^+−ethynol complex is the attachment of the metal to the terminal C atom of CHCOH, whereas the quartet counterpart favors a CC π-type bound structure. The peculiar stability of the quartet state (lying at −64.4 kcal/mol or being 18.0 kcal/mol more stable than **^{6}4**) suggests that the π-type bonding stabilizes the species largely. Correspondingly, in this case ethynol suffers relatively large structural change upon complexation. Mulliken atomic spin densities are found to be populated mostly on Fe^+ in both cases (4.90 and 3.23 for the sextet and quartet states, respectively; see Supporting Information Table S2). NBO analysis of the sextet complex shows that the terminal C atom forms only one β singly occupied σ binding orbital with Fe^+ instead of the second $\beta-\pi$ orbital with the inner C as for free CHCOH (see Supporting Information Table S3). The adduct is stabilized by electron donation of $4s(Fe^+) \rightarrow \pi^*(CC)$ and $\sigma(Fe^+C^2) \rightarrow 2s2p^{4.16}(C^1)$ as well as back-donation of $2s2p^{4.16}(C^1) \rightarrow \sigma^*(Fe^+C^2)$ ($\Delta E^{(2)} = 67.0$ kcal/mol; see Supporting Information Table S4). In the quartet state (**4**), however, the rupture of the $\beta-\pi(CC)$ orbital is favorable for formation of the β singly occupied σ binding orbitals of Fe^+ with both C atoms. In addition, this later attachment favors relatively strong donor−acceptor interaction between Fe^+ and CHCOH ($\Delta E^{(2)} = 147.1$ kcal/mol). All these facts suggest the stability as well as the large structural change of ethynol for the quartet species. The transition state (**TS_{3-4}**) for this possibility on the respective sextet and quartet pathways lies at 17.7 and 22.3 kcal/mol below the energetic zero. Nonreactive dissociation of Fe^+−ethynol would account for the $Fe^+(^6D)$- and $Fe^+(^4F)$-regenerated product, ethynol, with the overall exothermicities of 13.1 or 0.7 kcal/mol, respectively.

An inspection of both high- and low-spin PESs in Figure 3 shows that this product channel may experience four crossings, i.e., immediately before and after the encounter association, before the ligands coupling, and at the product exit.

3.3.3. Cyclization. The sextet and quartet PESs together with the schematic structures involved in the reaction pathways are shown in Figure 4. Information about the relevant species in their sextet and quartet states is given in Supporting Information Figures S3 and S4, respectively.

Following the formation of **2**, alternatively, an intramolecular rearrangement of FeO^+ stabilizing the system by 20.0 and 12.1 kcal/mol would yield "metallaoxacyclobutene" species *c*-$CHCHOFe^+$ (**5**) on the respective sextet and quartet surfaces; the activation energies for this process are calculated to be 14.2 and 11.9 kcal/mol. Once the "metallaoxacyclobutene" is formed, four possible pathways would be immediately followed, that

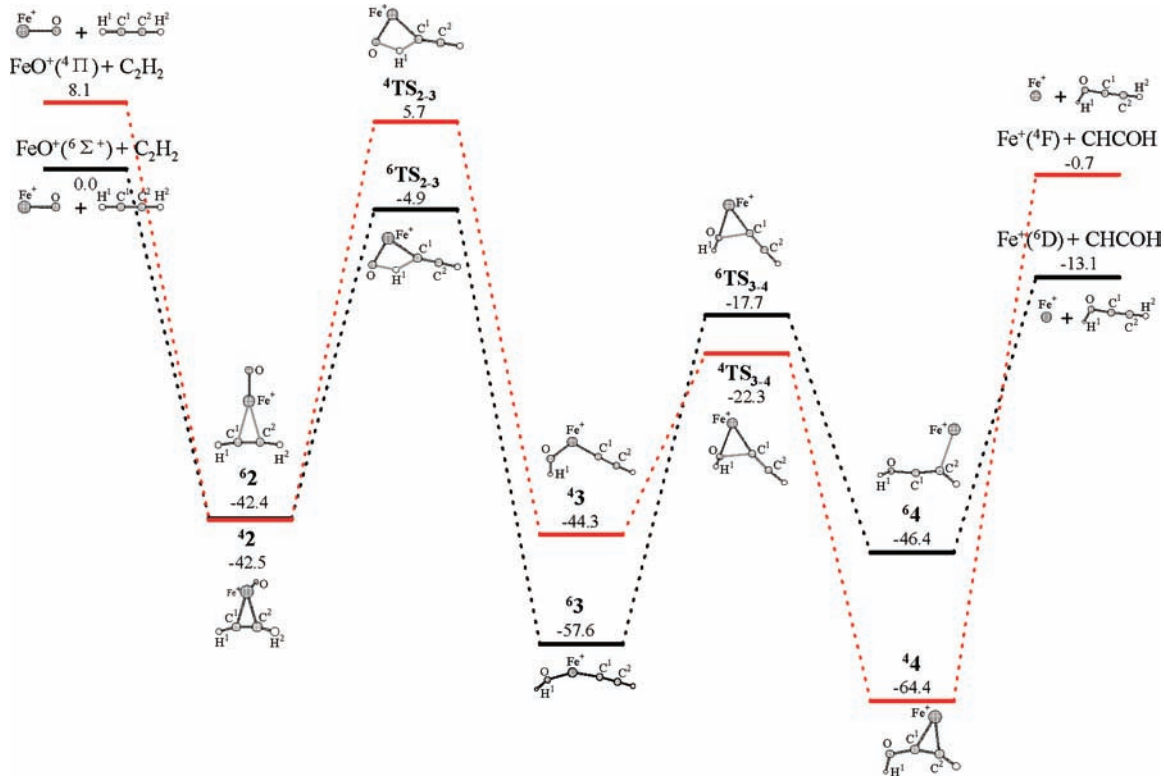

Figure 3. Energy profile for C_2H_2 oxidation by FeO^+ involving the direct hydrogen-abstraction mechanism. Numbers refer to the relative stabilities (in kcal/mol) with respect to the separated reactants of $C_2H_2 + FeO^+(^6\Sigma^+)$ evaluated at the B3LYP/DZVP(opt+3f)+6-311+G(2d,2p) level including ZPE corrections. Scaling factor for the ZPE is 0.961.

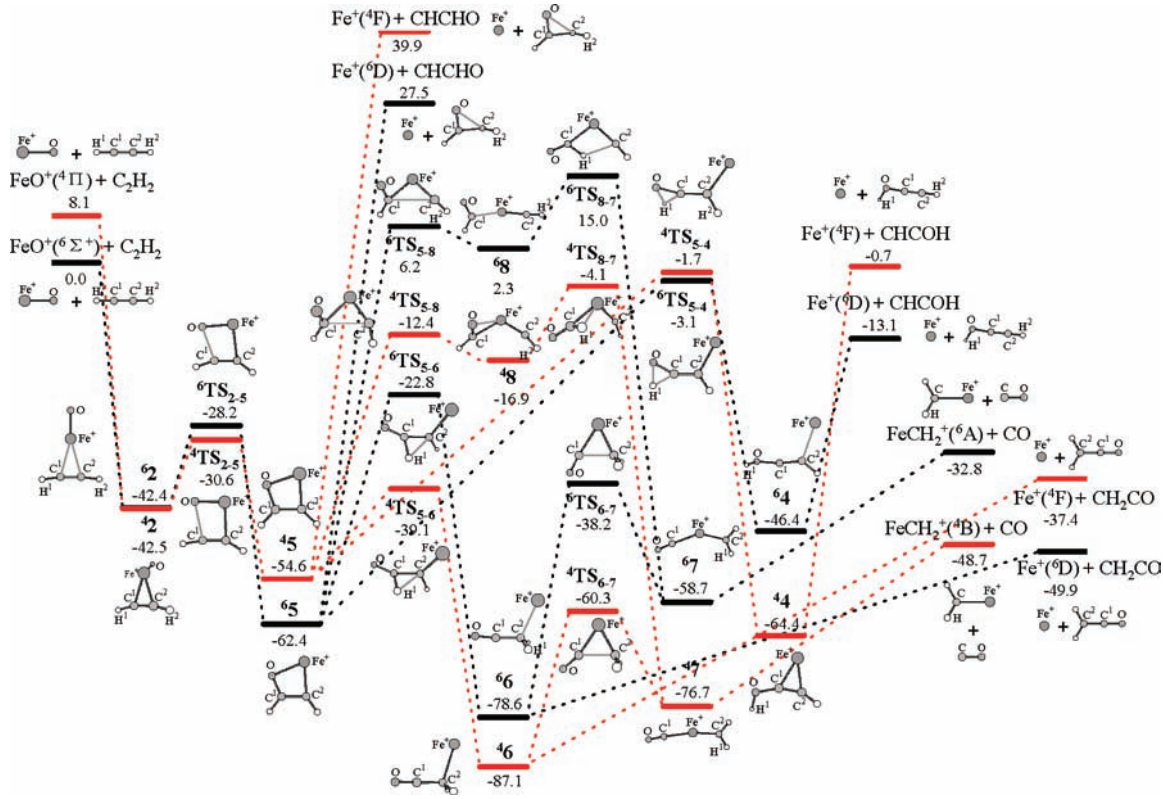

Figure 4. Energy profile for C_2H_2 oxidation by FeO^+ associated with the cyclization mechanism. Parameters follow the same notations as in Figure 3.

is, (i) direct dissociation, (ii) C−C insertion, (iii) C-to-O hydrogen shift, and/or (iv) C-to-C hydrogen shift.

We can find from Figure 4 that the first pathway from species **5** involving direct decomposition of Fe^+−(CHCHO) accounts for formylcarbene + Fe^+, but this is a strongly endothermic channel on both the high- and low-spin surfaces.

For the C−C insertion pathway, as shown in Figure 4, insertion of Fe^+ into the HC−CHO bond would account for

C−C insertion species **8**. The relevant transition state (**TS_{5-8}**) in its sextet and quartet states is located at 6.2 and −12.4 kcal/mol relative to the energetic zero, respectively. The new species can also be explained as the dicoordination of Fe^+ (with the CH and OCH groups) as for species **3**. Furthermore, the quartet species is also featured by an OC π-type bound structure of the metal with OCH. However, in this case the quartet state (E_{rel} = −16.9 kcal/mol) is indeed more stable than the sextet state (E_{rel} = 2.3 kcal/mol) rather than the reverse order as for **3**. Mulliken atomic spin densities in the high-spin species are populated extensively on Fe^+, O, and C^2 atoms (3.88, 0.44, and 0.38; see Supporting Information Table S2). NBO analysis detects that covalent bonds are only formed between Fe^+ and CH via one double occupied σ and two β-single occupied π binding orbitals (see Supporting Information Table S3) and the complex is favored by donor−acceptor interactions between Fe^+CH and OCH entities ($\Delta E^{(2)}$ = 54.3 kcal/mol; see Supporting Information Table S4). In the quartet state, however, Mulliken atomic spin densities mainly concentrate on Fe^+ and C^2 (3.50 and −0.73); the rupture of a β-single occupied $\pi(C^1O)$ orbital is compensated by one more $\alpha-\pi(Fe^+C^2)$ as well as two β-single occupied $\sigma(Fe^+C^1)$ and $\sigma(Fe^+O)$ binding orbitals (see Supporting Information Table S3), explaining the relatively large stabilization of this state. Afterward, a direct hydrogen migration from OCH to CH would convert the system into complex **7**, which has an analogous dicoordinated structure with the same excited- and ground-state order as its direct precursor **8**. Transition state for this process (**TS_{8-7}**) constitutes the highest energy point along the whole reaction coordinate, lying at 15.0 kcal/mol for the sextet and −4.1 kcal/mol for the quartet. For the new species, NBO analysis shows that Fe^+ forms strong covalent bonds with CH_2, whereas the binding of Fe^+−CO is dominated by donor−acceptor stabilization and thus is relatively weak. Therefore, **7** would release CO and $FeCH_2^+$ easily using the internal energy acquired. The overall reaction to yield $FeCH_2^+$(^{6}A or ^{4}B) + CO is an exothermic process with a reaction heat of 32.8 or 48.7 kcal/mol.

The third possible exit of species **5** involves a direct C^1-to-O hydrogen shift giving complex **4**, which is assisted by stretch of the Fe^+O bond. This possibility involves transition state **TS_{5-4}** with activation energies of more than 50 kcal/mol in both states, but they still lie at 2−3 kcal/mol below the energetic zero. Regeneration of Fe^+ giving ethynol from **4** has been discussed above.

Along the last and most important pathway, i.e., C-to-C hydrogen shift, a direct H migration from C^1 to C^2 would carry complex **5** to the Fe^+−ketene adduct (**6**). This possibility involves transition state **TS_{5-6}**, lying at −22.8 and −39.1 kcal/mol, respectively, for its sextet and quartet states. Similar to **4**, the new species also presents a Fe^+−ligand structure, in which the metal attaches at the CH_2 end of ketene with the Fe^+−C distances of 2.320 and 2.018 Å, respectively (see Figure 4 and Supporting Information Figures S3 and S4). Irrespective of the multiplicities, the new species is much more stable, with also the quartet state being the ground state (E_{rel} = −78.6 kcal/mol for high spin and −87.1 kcal/mol for low spin).

One exit of species **6** is direct rupture of the Fe^+−C bond accounting for the final products of Fe^+(^{6}D or ^{4}F) + CH_2CO, which is exothermic by 49.9 or 37.4 kcal/mol with respect to the energetic zero. The other exit channel for the species is insertion of the metal into the C−C bond of ketene to form the rather stable CH_2-Fe^+-CO (**7**). This possibility involves transition state **TS_{6-7}** with activation energies of 40.4 and 26.8 kcal/mol for the sextet and quartet reaction pathways, respectively. Species **7** would eventually dissociate into the $FeCH_2^+$ + CO products as mentioned above.

Inspection of Figure 4 shows that the formation of $FeCH_2^+$ and CO should be characterized by three spin inversions, which occur at the entrance channel and immediately before and after immediate **5**, respectively, entailing that the reaction is a spin-forbidden process with the reactants having a sextet state and products in the quartet state. Besides, the reaction to yield Fe^+ and C_2H_2O proceeds the forth more crossing at the exit channel and ultimately produces the sextet products. However, it is well-known that in general spin inversion in transition metal containing systems only has a certain degree of efficiency[21,44] so that the probability of the reaction proceeding on the respective sextet and quartet surfaces could not be negligible considering the energetics.

3.4. $FeCH_2^+$ Reduction by N_2O. The PES together with schematic structures involved in the sextet and quartet reaction pathways is shown in Figure 5, and information about these species is given in Supporting Information Figure S5. Irrespective of its electronic state, ^{4}B or ^{6}A, $FeCH_2^+$ reacts with N_2O giving the $(CH_2)Fe^+(N_2O)$ adduct (**9**), which lies at −25.1 kcal/mol for the quartet with respect to the quartet reactants or −6.5 kcal/mol for the sextet. Once the new adduct is formed, N_2 would be ejected to form the $OFeCH_2^+$ oxide through exit barrier **TS_9** that lies at 15.2 kcal/mol on the sextet surface and −0.7 kcal/mol for the quartet process. The shortening of the metal−oxygen bond as well as the lengthening of the O−N bond in the transition state suggest it is really ready for dissociation into N_2 + $OFeCH_2^+$. A subsequent rearrangement of the $OFeCH_2^+$ oxide would account for the very stable Fe^+−formaldehyde complex, lying at −89.5 and −87.7 kcal/mol in its quartet and sextet states, respectively. This possibility involves "early" transition states with the activation energies of 8.5 and 1.5 kcal/mol for the quartet and sextet, respectively. Finally, a barrier-free dissociation of Fe^+-OCH_2 would yield Fe^+ (^{4}F or ^{6}D) + OCH_2 + N_2, exothermic by 40.4 or 52.9 kcal/mol for the overall reaction. As shown in Figure 5, a crossing between the high- and low-spin PESs taking place in the last step indicates this reaction may be also a spin-forbidden process.

3.5. Fe^+-Catalyzed Oxidation of C_2H_2 by N_2O. Now, we consider the energetics for the overall Fe^+-catalyzed oxidation of C_2H_2 by N_2O. Gas-phase experimental studies by Kappes and Staley inferred that this catalytic reaction produces C_2H_2O, CH_2O, CO, and N_2 via both two-step and three-step catalytic cycles (reactions 1–4) with an estimated C_2H_2O/CO branching ratio of 1:1.[9]

Let us consider the energetics along the ground-state pathway. The O-atom transport generating FeO^+($^6\Sigma^+$) is 35.9 kcal/mol exothermic (reaction 6). Because of a double spin inversion, the transition state for this process is below the energetic zero. Once FeO^+ is formed, acetylene could be oxidized by FeO^+ and partly convert via different mechanisms to ketene (CH_2CO), ethynol (CHCOH), and formylcarbene (CHCHO) with 85.8, 49.0, and 8.4 kcal/mol exothermicities, respectively (reactions 7a–7c). Also, it produces $FeCH_2^+$ and CO, exothermic by 84.6 kcal/mol (reaction 8). Oxidations to ketene and CO are strongly favorable because of the strong exothermicity of both channels as well as no high-lying transition states along the product pathway (cyclization−C-to-C hydrogen shift). This situation agrees well with the ICR experimental findings, in which the branching ratio of CO and C_2H_2O losses is approximately 1:1.[9] Finally, a strongly further exothermic reaction with N_2O could regenerate Fe^+ readily from the CO loss partner $FeCH_2^+$ (reaction 9). The overall three-step Fe^+-catalyzed oxidation of

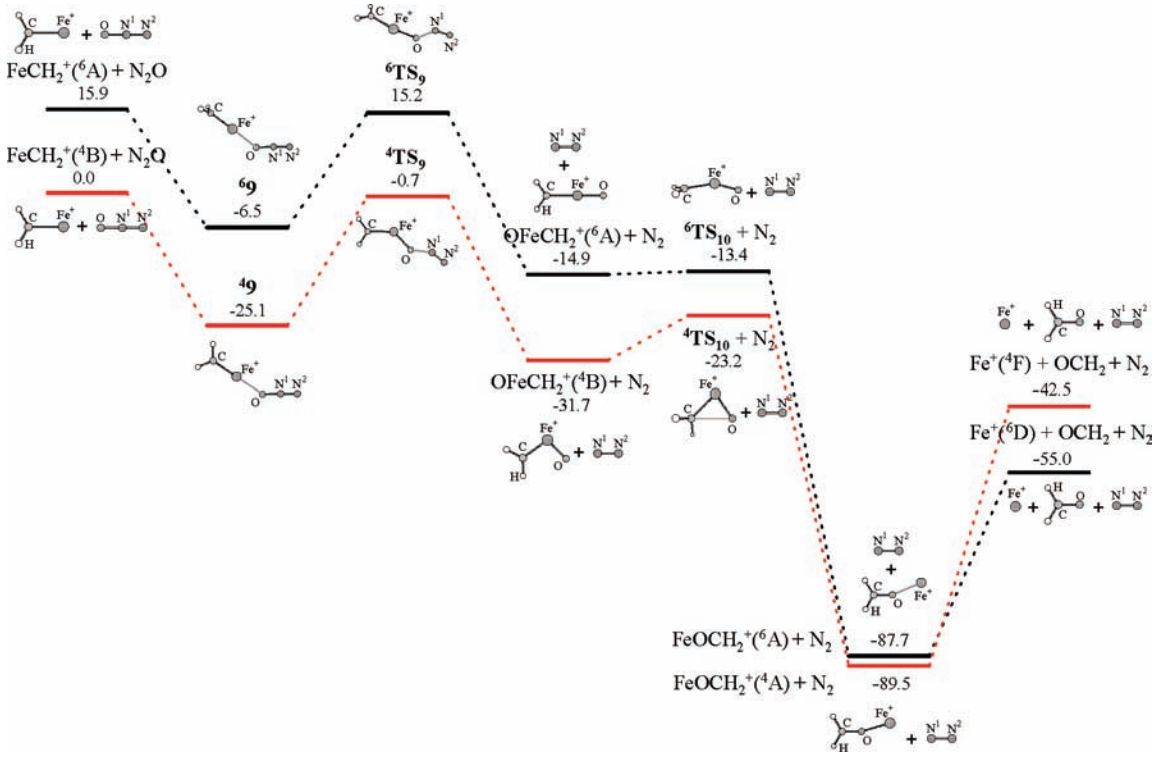

Figure 5. Energy profile for $FeCH_2^+$ reduction by N_2O. Numbers refer to the relative stabilities (in kcal/mol) with respect to the separated reactants of N_2O + $FeCH_2^+(^4B)$ evaluated at the B3LYP/DZVP(opt+3f)+6-311+G(2d,2p) level including ZPE corrections. Scaling factor for the ZPE is 0.961.

acetylene by two N_2O molecules to form CO and formaldehyde (reaction 9) is calculated to be exothermic by 139.6 kcal/mol.

$$N_2O + Fe^+(^6D) \rightarrow FeO^+(^6\Sigma^+) + N_2 + 35.9 \text{ kcal/mol} \quad (6)$$

$$N_2O + Fe^+(^6D) + C_2H_2 \rightarrow Fe^+(^6D) + CH_2CO + N_2 + 85.8 \text{ kcal/mol} \quad (7a)$$

$$\rightarrow Fe^+(^6D) + CHCOH + N_2 + 49.0 \text{ kcal/mol} \quad (7b)$$

$$\rightarrow Fe^+(^6D) + CHCHO + N_2 + 8.4 \text{ kcal/mol} \quad (7c)$$

$$\rightarrow FeCH_2^+(^4B) + CO + N_2 + 84.6 \text{ kcal/mol} \quad (8)$$

$$2N_2O + Fe^+(^6D) + C_2H_2 \rightarrow Fe^+(^6D) + 2N_2 + CO + OCH_2 + 139.6 \text{ kcal/mol} \quad (9)$$

4. Conclusions

We have elucidated the mechanism of the Fe^+-mediated oxidation of acetylene by N_2O, which involves both two- and three-step catalytic cycles in the gas phase.

Fe^+ reaction with N_2O generating FeO^+ occurs through a direct O-abstraction mechanism on the sextet PES, and a N−O insertion mechanism is favorable for the quartet pathway. Considering spin inversions, the rate-determining energy barrier for this process is located below the entrance channel and the overall reaction is 35.9 kcal/mol exothermic.

In the second step of the catalytic cycles, two mechanisms corresponding to direct hydrogen abstraction and cyclization could take place following association of acetylene with the nascent FeO^+. The former mechanism accounting for ethynol formation corresponds to a direct acetylenic H abstraction by the oxide O with the upmost activation barrier below the entrance channel by about 5 kcal/mol. The other mechanism involving a cyclization to form a "metallaoxacyclobutene" structure is followed by four possible pathways, i.e., direct dissociation (for producing formylcarbene), C−C insertion (for products ketene and carbon monoxide), C-to-O hydrogen shift (for ethynol), and/or C-to-C hydrogen shift (for ketene and carbon monoxide). The overall exothermicity values of products carbon monoxide, ketene, ethynol, and formylcarbene are 84.6, 85.8, 49.0, and 8.4 kcal/mol, respectively. The strong exothermicities as well as energetically low location of the intermediates suggest oxidation to ketene and carbon monoxide along the cyclization−C-to-C hydrogen shift pathway is the most favorable. This situation agrees well with the ICR experiment, where a branching ratio of about 1:1 was estimated for CO and C_2H_2O losses. In this step, spin inversions could be not very important due to the low location of both PESs with different spin multiplicities.

Reduction of the CO loss partner $FeCH_2^+$ by another N_2O molecule constitutes the third step of the catalytic cycle, which involves a direct abstraction of O atom from N_2O giving $OFeCH_2^+$ and then an intramolecular rearrangement to form formaldehyde adduct Fe^+-OCH_2. Considering the energy acquired from the initial reactants, this reaction is also energetically favored and the overall oxidation of acetylene by two N_2O molecules to CO and formaldehyde is exothermic by 139.6 kcal/mol. Spin inversion may take place in the exit channel of the process.

Acknowledgment. This work was supported by SRF for ROCS, NCET-05-0608, and the Excellent Young Teachers Program of MOE, PRC, the National Natural Science Foundation of China (20476061), the Natural Science Foundation of Shandong Province, PRC (Y2006B35), and the State Key Basic Research Program of PRC (2006CB202505).

Supporting Information Available: Optimized geometries, selected structural parameters, calculated energies, zero-point

energies, $\langle S^2 \rangle$, Mulliken atomic spin densities, and results of NBO analysis for all species involved in the Fe^+-catalyzed oxidation of acetylene by N_2O. This material is available free of charge via the Internet at http://pubs.acs.org.

References and Notes

(1) (a) Torrent, M.; Solà, M.; Frenking, G. *Chem. Rev.* **2000**, *100*, 439. (b) Niu, S.; Hall, M. B. *Chem. Rev.* **2000**, *100*, 353.

(2) Eller, K.; Schwarz, H. *Chem. Rev.* **1991**, *91*, 1121.

(3) Weisshaar, J. C. *Acc. Chem. Res.* **1993**, *26*, 213.

(4) Böhme, D. K.; Schwarz, H. *Angew. Chem., Int. Ed.* **2005**, *44*, 2336.

(5) Kapteijn, F.; Rodriguez-Mirasol, J.; Moulijn, J. A. *Appl. Catal., B* **1996**, *9*, 25.

(6) (a) Armentrout, P. B.; Halle, L. F.; Beauchamp, J. L. *J. Chem. Phys.* **1982**, *76*, 2449. (b) Kretzschmar, H.; Fiedler, A.; Harvey, J. N.; Schröder, D.; Schwarz, H. *J. Phys. Chem. A* **1997**, *101*, 6252. (c) Lavrov, V. V.; Blagojevic, V.; Koyanagi, G. K.; Orlova, G.; Bohme, D. K. *J. Phys. Chem. A* **2004**, *108*, 5610.

(7) (a) Delabie, A.; Pierloot, K. *J. Phys. Chem. A* **2002**, *106*, 5679. (b) Martínez, A.; Goursot, A.; Coq, B.; Delahay, G. *J. Phys. Chem. B* **2004**, *108*, 8823. (c) Solans-Monfort, X.; Sodupe, M.; Branchadell, V. *Chem. Phys. Lett.* **2003**, *368*, 242. (d) Yang, X. Y.; Wang, Y. C.; Geng, Z. Y.; Liu, Z. Y. *Chem. Phys. Lett.* **2006**, *430*, 265. (e) Lü, L. L.; Liu, X. W.; Wang, Y. C.; Wang, H. Q. *J. Mol. Struct. (THEOCHEM)* **2006**, *774*, 59.

(8) Lias, S. G.; Bartmess, J. E.; Liebmann, J. F.; Holmes, J. L.; Levin, R. D.; Mallard, W. G. *J. Phys. Chem. Ref. Data* **1988**, *17*, Suppl 1.

(9) Kappes, M. M.; Staley, R. H. *J. Am. Chem. Soc.* **1981**, *103*, 1286.

(10) Schröder, D.; Schwarz, H. *Angew. Chem., Int. Ed. Engl.* **1990**, *29*, 1431.

(11) Schröder, D.; Schwarz, H. *Angew. Chem., Int. Ed. Engl.* **1990**, *29*, 1433.

(12) Schwarz, H. *Angew. Chem., Int. Ed. Engl.* **1991**, *30*, 820.

(13) Ryan, M. F.; Stöckigt, D.; Schwarz, H. *J. Am. Chem. Soc.* **1994**, *116*, 9565.

(14) Ryan, M. F.; Fiedler, A.; Schröder, D.; Schwarz, H. *Organometallics* **1994**, *13*, 4072.

(15) Ryan, M. F.; Fiedler, A.; Schröder, D.; Schwarz, H. *J. Am. Chem. Soc.* **1995**, *117*, 2033.

(16) Schröder, D.; Schwarz, H. *Angew. Chem., Int. Ed. Engl.* **1995**, *34*, 1973.

(17) Baranov, V.; Javahery, G.; Hopkinson, A. C.; Bohme, D. K. *J. Am. Chem. Soc.* **1995**, *117*, 12801.

(18) Blagojevic, V.; Orlova, G.; Bohme, D. K. *J. Am. Chem. Soc.* **2005**, *127*, 3545.

(19) Rondinelli, F.; Russo, N.; Toscano, M. *Inorg. Chem.* **2007**, *46*, 7489.

(20) Chiodo, S.; Russo, N.; Sicilia, E. *J. Comput. Chem.* **2005**, *26*, 175.

(21) (a) Danovich, D.; Shaik, S. *J. Am. Chem. Soc.* **1997**, *119*, 1773. (b) Filatov, M.; Shaik, S. *J. Phys. Chem.* **1998**, *102*, 3835. (c) Fiedler, A.; Schröder, D.; Shaik, S.; Schwarz, H. *J. Am. Chem. Soc.* **1994**, *116*, 10734. (d) Shaik, S.; Danovich, D.; Fiedler, A.; Schröder, D.; Schwarz, H. *Helv. Chim. Acta* **1995**, *78*, 1393.

(22) (a) Yoshizawa, K.; Shiota, Y.; Yamabe, T. *J. Am. Chem. Soc.* **1998**, *120*, 564. (b) Yoshizawa, K.; Shiota, Y.; Yamabe, T. *J. Chem. Phys.* **1999**, *111*, 538. (c) Shiota, Y.; Yoshizawa, K. *J. Am. Chem. Soc.* **2000**, *122*, 12317. (d) Shiota, Y.; Yoshizawa, K. *J. Chem. Phys.* **2003**, *118*, 5872. (e) Yoshizawa, K.; Shiota, Y.; Kagawa, Y.; Yamabe, T. *J. Phys. Chem. A* **2000**, *104*, 2552.

(23) (a) Yoshizawa, K.; Kagawa, Y. *J. Phys. Chem. A* **2000**, *104*, 9347. (b) Yumura, T.; Amenomori, T.; Kagawa, Y.; Yoshizawa, K. *J. Phys. Chem. A* **2002**, *106*, 621.

(24) (a) Yoshizawa, K.; Shiota, Y.; Yamabe, T. *J. Am. Chem. Soc.* **1999**, *121*, 147. (b) Shiota, Y.; Suzuki, K.; Yoshizawa, K. *Organometallics* **2005**, *24*, 3532.

(25) Harris, N.; Shaik, S.; Schröder, D.; Schwarz, H. *Helv. Chim. Acta* **1999**, *82*, 1784.

(26) (a) Stephens, P. J.; Devlin, F. J.; Chabalowski, C. F.; Frisch, M. J. *J. Phys. Chem.* **1994**, *98*, 11623. (b) Becke, A. D. *J. Chem. Phys.* **1993**, *98*, 5648. (c) Lee, C.; Yang, W.; Parr, R. G. *Phys. Rev. B* **1988**, *37*, 785. (d) Salahub, D. R. *The Challenge of d and f Electrons*; Zerner, M. C. Ed.; American Chemical Society: Washington, DC, 1989. (e) Parr, R. G.; Yang, W. *Density-Functional Theory of Atoms and Molecules*; Oxford University Press: Oxford, 1989.

(27) Frisch, M. J.; Trucks, G. W.; Schlegel, H. B.; Scuseria, G. E.; Robb, M. A.; Cheeseman, J. R.; Montgomery, J. A., Jr.; Vreven, T.; Kudin, K. N.; Burant, J. C.; Millam, J. M.; Iyengar, S. S.; Tomasi, J.; Barone, V.; Mennucci, B.; Cossi, M.; Scalmani, G.; Rega, N.; Petersson, G. A.; Nakatsuji, H.; Hada, M.; Ehara, M.; Toyota, K.; Fukuda, R.; Hasegawa, J.; Ishida, M.; Nakajima, T.; Honda, Y.; Kitao, O.; Nakai, H.; Klene, M.; Li, X.; Knox, J. E.; Hratchian, H. P.; Cross, J. B.; Adamo, C.; Jaramillo, J.; Gomperts, R.; Stratmann, R. E.; Yazyev, O.; Austin, A. J.; Cammi, R.; Pomelli, C.; Ochterski, J. W.; Ayala, P. Y.; Morokuma, K.; Voth, G. A.; Salvador, P.; Dannenberg, J. J.; Zakrzewski, V. G.; Dapprich, S.; Daniels, A. D.; Strain, M. C.; Farkas, O.; Malick, D. K.; Rabuck, A. D.; Raghavachari, K.; Foresman, J. B.; Ortiz, J. V.; Cui, Q.; Baboul, A. G.; Clifford, S.; Cioslowski, J.; Stefanov, B. B.; Liu, G.; Liashenko, A.; Piskorz, P.; Komaromi, I.; Martin, R. L.; Fox, D. J.; Keith, T.; Al-Laham, M. A.; Peng, C. Y.; Nanayakkara, A.; Challacombe, M.; Gill, P. M. W.; Johnson, B.; Chen, W.; Wong, M. W.; Gonzalez, C.; Pople, J. A. *Gaussian 03*, revision B.05; Gaussian, Inc.: Pittsburgh, PA, 2003.

(28) Frisch, M. J.; Pople, J. A.; Binkley, J. S. *J. Chem. Phys.* **1984**, *80*, 3265.

(29) (a) Seeger, R.; Pople, J. A. *J. Chem. Phys.* **1977**, *66*, 3045. (b) Bauernschmitt, R.; Ahlrichs, R. *J. Chem. Phys.* **1996**, *104*, 9047.

(30) (a) Glendening, E. D.; Reed, A. E.; Carpenter, J. E.; Weinhold, F. NBO Version 3.1. (b) Reed, A. E.; Curtiss, L. A.; Weinhold, F. *Chem. Rev.* **1988**, *88*, 899. (c) Foster, J. P.; Weinhold, F. *J. Am. Chem. Soc.* **1980**, *102*, 7211.

(31) Elkind, J. L.; Armentrout, P. B. *J. Am. Chem. Soc.* **1986**, *108*, 2765.

(32) Fiedler, A.; Schröder, D.; Schwarz, H.; Tjelta, B. L.; Armentrout, P. A. *J. Am. Chem. Soc.* **1996**, *118*, 5047.

(33) Schultz, R. H.; Armentrout, P. B. *J. Phys. Chem.* **1993**, *97*, 596.

(34) *Organometallic Ion Chemistry*; Freiser, B. S., Ed.; Kluwer: Dordrecht, The Netherlands, 1996.

(35) Schultz, R. H.; Crellin, K. C.; Armentrout, P. B. *J. Am. Chem. Soc.* **1991**, *113*, 8590.

(36) Fisher, E. R.; Schultz, F. R.; Armentrout, P. B. *J. Phys. Chem.* **1989**, *93*, 7382.

(37) Armentrout, P. B.; Sunderlin, L. S.; Fisher, E. R. *Inorg. Chem.* **1989**, *28*, 4437.

(38) Tjelta, B. L.; Walter, D.; Armentrout, P. B. *Int. J. Mass Spectrom.* **2001**, *204*, 7.

(39) Sugar, J.; Corliss, C. *J. Phys. Chem. Ref. Data* **1985**, *14*, 1.

(40) Fowler, J. E.; Galbraith, J. M.; Vacek, G.; Schaefer, H. F. *J. Am. Chem. Soc.* **1994**, *116*, 9311.

(41) Vacek, G.; Galbraith, J. M.; Yamaguchi, Y.; Schaefer, H. F.; Nobes, R. H.; Scott, A. P.; Radom, L. *J. Phys. Chem.* **1994**, *98*, 8660.

(42) Girard, Y.; Chaquin, P. *J. Phys. Chem.* **2003**, *98*, 8660.

(43) (a) Dewar, M. J. S. *Bull. Soc. Chim. Fr.* **1951**, *C79*, 18. (b) Chatt, J.; Duncansom, L. A. *J. Chem. Soc.* **1953**, 2939. (c) Gerloch, M.; Constable, E. C. *Transition Metal Chemistry*; VCH: New York, 1994; Chapter 6.5.

(44) (a) Schwarz, H. *Int. J. Mass Spectrom.* **2004**, *237*, 75. (b) Schröder, D.; Shaik, S. Schwarz, H. *Acc. Chem. Res.* **2000**, *33*, 139.

JP800511H